Supplementary Information

Relating Energy Level Alignment and Amine-Linked Single Molecule Junction Conductance

M. Dell'Angela[1,2], G. Kladnik[3], A. Verdini[1], M. Kamenetska[4], I. Tamblyn[5], S.Y. Quek[5], J.B. Neaton[5], D. Cvetko[3], A. Morgante[1,2], L. Venkataraman[4]

[1]CNR-INFM Laboratorio Nazionale TASC, Basovizza SS-14, km 163.5, I-34012 Trieste, Italy,
[2]Department of Physics, University of Trieste, Trieste, Italy,
[3]Dept. of Physics, University of Ljubljana, Ljubljana, Slovenia,
[4]Dept. of Applied Physics and Applied Math., Columbia University, New York, NY,
[5]Molecular Foundry, Lawrence Berkeley National Laboratory, Berkeley, CA

morgante@tasc.infm.it; jbneaton@lbl.gov; lv2117@columbia.edu

Content:

Surface Preparation and Helium Scattering

The experiments have been carried out in ultra-high vacuum (UHV) conditions at the HASPES/ALOISA beamline (Elettra Synchrotron, Trieste)[1, 2] where it is possible to perform Helium Atom Scattering measurements and Photoemission Spectroscopy measurements by using helium discharge lamp or synchrotron light. Au(111) and Au(110) single crystals were obtained from Surface Preparation Laboratory (Denmark) and had a mis-cut of less than ±0.1 degrees, as confirmed with grazing incidence x-ray diffraction.

The Au(111) surface was prepared in situ by repeated cycles of Ar^+ sputtering at an energy of 1 keV, followed by annealing at temperatures of 700K. The Au(110) surface was prepared in situ by repeated cycles of Ar^+ sputtering at an energy of 1 keV, followed by annealing at temperatures of 800K, at which the (1x2) missing row reconstruction forms (see SI Figure S1)[3]. The herringbone reconstruction of Au(111) and the (1x2) missing row reconstruction of Au(110) have been checked by means of helium atom diffraction measurements and/or reflection high-energy electron diffraction (RHEED). The chemical cleanliness of the samples prior to molecule deposition was determined by means of X-Ray Photoemission Spectroscopy measurements, where carbon and nitrogen signals were found to be below the detection limit.

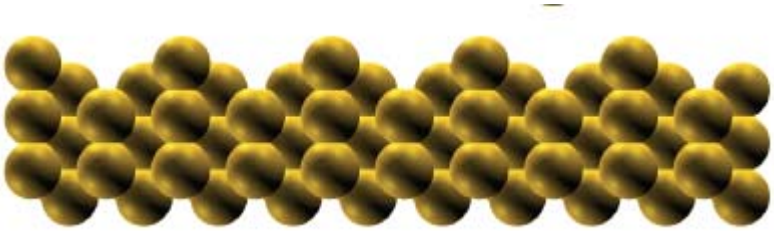

SI Figure S1 Au(110) surface structure showing the missing row reconstruction.

To characterize the surface, we first carried out temperature dependent Helium atom scattering measurements at the HASPES experimental chamber to determine the required coverage and deposition conditions for a monolayer or submonolayer of each of the molecules on Au(111) substrate. All the molecules (**TMBDA**, **BDA**, **TFBDA**) were deposited by sublimation, as purchased and with no further purification. During the deposition, the sample was kept at 270 K and the pressure in the experimental chamber due to the molecules rose to 10^{-7} mbar from a base pressure of about 10^{-9} mbar. We monitored the HAS specular beam intensity during the deposition, which exhibited a strong reduction. HAS is ideally suited to study the growth of organic thin films since it is a non-destructive, long-range order probe, extremely sensitive to the presence of uncorrelated defects such as adsorbed molecules.[4]. Strong reduction of the specular reflectivity (of the order of 10^{-3}-10^{-4} times the initial value) indicates that the surface is almost completely covered with molecules[5]. In fact, organic molecules on crystalline substrates are highly disordered scatterers for the Helium atoms, mainly because the Debye-Waller factor is particularly high for molecular vibrations and the molecules can adopt several geometrical configurations on the surface. Therefore helium atoms scattered from the organic layer contribute to diffuse and inelastic scattering, which both lead to the attenuation of the specular peak. Thermal desorption of molecules from the

organic films was subsequently measured by monitoring the He specular reflectivity as a function of the sample temperature. We show, in SI Figure 1, the first part of the He specular reflectivity curves, normalized to the specular intensity of the clean Au surface for **TMBDA**, **BDA** and **TFBDA** molecular films on Au(111). (See Figure 1 in the main text for full figure). The Helium specular peak intensity recovered 1% of the maximum value at the temperatures of 300 K, 270 K, 260 K for **TMBDA**, **BDA** and **TFBDA** respectively which have been used as monolayer temperatures. The same deposition conditions were then used in the ALOISA chamber to create monolayers of the molecules on either the Au(111) or the Au(110) surface.

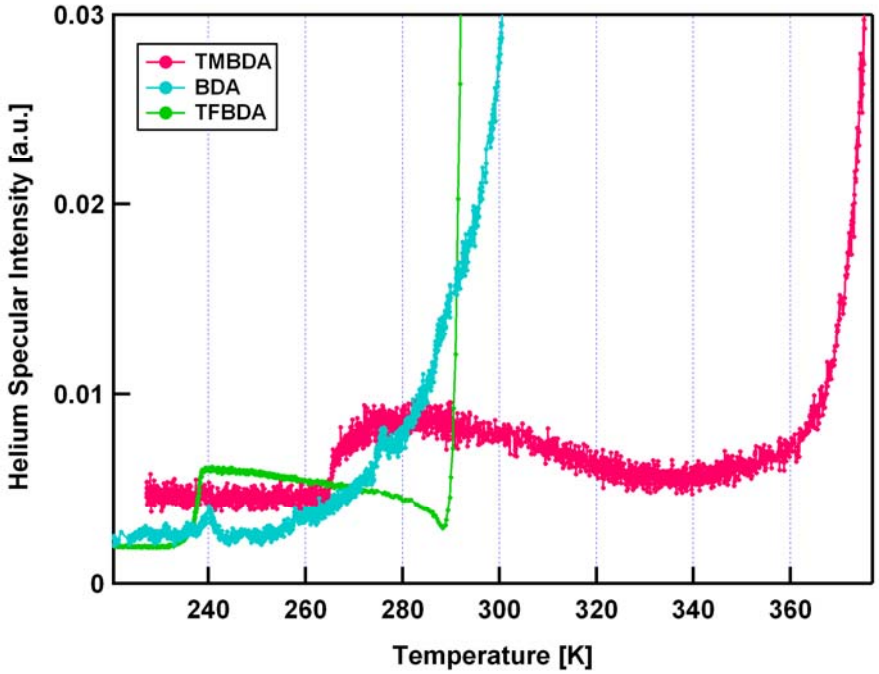

SI Figure S2 Helium specular reflectivity curves as a function of the sample temperature (heating rate 6±2 K/min), normalized to the specular intensity of the clean Au surface for **TMBDA**, **BDA** and **TFBDA** molecular films on Au(111).

On Au(110) the deposition procedure was similar: molecules were deposited by sublimation at temperatures of 270 K, as described previously for Au(111), and the films were subsequently heated to 330 K and 450 K for **TMBDA** and **BDA** respectively. The temperatures required to desorb the molecules are higher on Au(110) with respect to the Au(111). This can be due to the stronger binding of the molecules to the surface (which contains atoms with lower coordination). The HAS specular reflectivity during desorption of a multilayer of **BDA** on the two surfaces is shown in SI Figure 2 and it is clear that molecules desorb at higher temperatures from Au(110) than on Au(111). From both desorption temperatures we can roughly estimate the ratio of the molecule adsorption energy on 110 to 111 to be 1.15

XPS and UPS measurement details

UPS measurements have been performed at the HASPES experimental chamber by using a He discharge lamp (hv=21.2eV) in normal emission conditions. The spectra were aligned to the Au Fermi level, which was determined from a fit to the data. In particular, before each molecular deposition a spectrum for the clean Au(111) surface was acquired

and fitted by using a step function to fit the Au Fermi level, a Voigt peak to fit the Au(111) surface state and three Voigt peaks to reproduce the sharp increase of the d states in the valence band of the clean Au(111) spectrum above 2eV. Subsequentely for each UPS spectra obtained from each film was fit with the step and three clean Au(111) peaks (which were constrained in width and position) and an additional peak to fit the molecular HOMO. The energy of the HOMO determined from this fit by using this fitting procedure is influenced to some extent by the way the clean Au(111) is fit and this uncertainty is included in the large error bar for the HOMO position. In fact, the main reason for performing XPS measurements under resonant conditions is to confirm the energy difference between the HOMO and E_F determined from UPS.

The XPS measurements were performed at the ALOISA experimental chamber. Valence band spectra were acquired for several photon energies between 284eV and 288eV. They were aligned to the Au Fermi level. Each valence band spectrum was then normalized by the incident photon flux. Moreover the valence band spectrum acquired at 284eV was subtracted from each spectrum in order to have only the resonant contribution to the XPS data. Figure 3b of the paper shows data after this subtraction, with hv=286.6 eV and 287 eV shown, which correspond for the considered molecules to the Carbon K-edge NEXAFS excitations from C1s to pi* states localized on the 1 and 4 Carbons. At these energies the HOMO peak for each molecule is strongly enhanced. Finally the resonant part of the valence band spectrum has been fitted by using gaussians of 1eV FWHM which account for the HOMO levels.

The large error bar in this case is due to the subtraction procedure and to the uncertainty in determining the Fermi Au level which is not very strong at these photon energies.

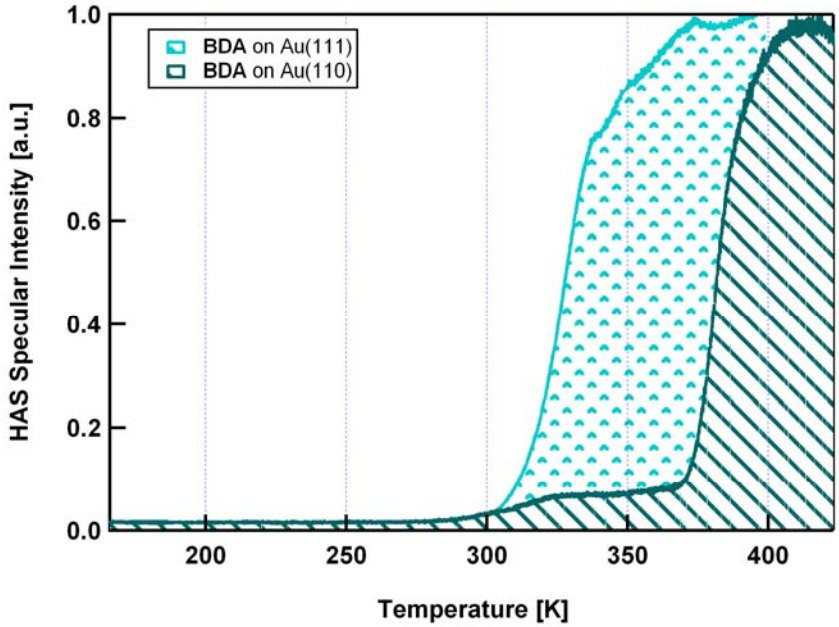

SI Figure S3 Helium specular reflectivity curves as a function of the sample temperature (heating rate 6±2 K/min), normalized to the specular intensity of the clean Au surface for **BDA** molecular films on Au(111) and Au(110).

Conductance Measurements

The results from conductance data reported in this work are taken from previous published work[6] and are reproduced here. This work was based on a method detailed in two earlier papers[7, 8], where conductance measurements of amine-linked molecules are carried out using the STM-break junction technique. Briefly, this technique relies on first breaking an Au-point contact in a solution of the target molecules. Conductance is measured as a function of electrode displacement, and plateaus are seen in conductance traces at integer multiples of the quantum of conductance, and at a molecule dependent value. When histograms are constructed from 20000 measurements, clear peaks are seen at integer multiples of G_0 as well as at a single value for these benzene derivatives. The position of the molecular conductance peak is determined by fitting a Lorentzian to the histogram peak, and the center value of the Lorentzian is quoted in Table 1 of the main text. Since molecular junctions are formed after breaking a gold point contact with a single Au atom bridging the tip and substrate, both the tip and substrate are very sharp prior to the formation of the single molecule junction, thus it is unlikely that two molecules can bridge the gap. The conductance data reported here is therefore for a *single* molecule junction.

Theoretical Procedures and Results

Geometry Determination:

Since the angle θ of the molecule relative to the surface is a relatively soft degree of freedom, we optimize adsorbate geometries by fixing the angle θ between the plane of the benzene ring and the surface (the Au-N-C angle) for several values of θ, allowing all other structural degrees of freedom to relax. Using this strategy to minimize energy with respect to θ, our optimum values for θ are 23°, 27°, and 54° for **TFBDA**, **BDA**, and **TMBDA**, with GGA-PBE molecule adsorption energies of 0.26 eV, 0.36 eV, and 0.44 eV, respectively. As mentioned in the text, these values differ from experiment presumably owing to the lack of van der Waals interactions in the PBE exchange-corrrelation functional used in this work. We also note that for **BDA**, small changes in angle, of θ ~ 20-45°, incur changes in binding energy that are within thermal fluctuations at room temperature. For **TFBDA** and **TMBDA**, similarly accessible angles range from θ ~ 15-50° and θ ~ 40-80°.

DFT+Σ approach

1. Self-energy term

The self-energy correction consists of two parts: first, a "bare" or "intramolecular" term, correcting for the difference between DFT HOMO and LUMO energies and the ionization potential (IP) and electron affinity (EA) of the gas-phase molecule computed from total energy differences (ΔSCF)[9]; and second, an "image-charge" term accounting for the effect of electrode polarization on the energy of the added electron (LUMO) or hole (HOMO)[10]. This self-energy has no adjustable parameters and is found to give an accurate description of quasi-particle level alignment for weakly coupled molecule−metal

substrate systems where the frontier orbitals are not significantly altered by coupling to the surface, where self-energy corrections for metallic states can be neglected, and where substrate-molecule dynamical correlation effects are negligible[10]. For weakly coupled molecular adsorbates, this method has been demonstrated to make accurate predictions for experimental measurements of conductance, G[11], as well as the exponential decay constant β that characterizes the change in conductance of molecular wires with length[12]. In order to determine the gas phase term, we perform ΔSCF calculations using a localized basis set (with the Gaussian package[13]) and a hybrid exchange-correlation functional (B3LYP [14, 15] ΔSCF with B3LYP results in ionization potentials (IPs) and electron affinities (EAs) for BDA which are in relatively good agreement with experiment. In Table 1 we show the components of the self-energy correction for molecules we studied.

Table 1:

Molecule (binding motif)	HOMO relative to E_F [eV]	Bare term [eV]	Image-charge term [eV]	Total self-energy [eV]
TFBDA	-0.5	-2.86	1.44	-1.4
BDA (clean 111)	-0.4	-2.73	1.31	-1.4
TMBDA	-0.1	-2.49	1.33	-1.2

Table 1: HOMO position relative to E_F as reported by DFT. Contributions to the self-energy due to the "bare" or "intramolecular" term and the "image-charge" term. The total self-energy is the sum of these two terms.

2. Calculation of HOMO energy level

This self-energy correction is added explicitly to the SIESTA Hamiltonian by an orbital-dependent term of the form $\hat{\Sigma} = \sum_n \Sigma_n \left|\psi_n^{mol}\right\rangle\left\langle\psi_n^{mol}\right|$, where $\left|\psi_n^{mol}\right\rangle$ denotes an eigenstate of the isolated molecule, and Σ_n is the self-energy correction for the nth molecular level. In the present study, for simplicity, we compute Σ_n for only the HOMO and LUMO, as described above, and apply Σ_{HOMO} to all occupied states, and Σ_{LUMO} to all unoccupied states. The modified Hamiltonian is then solved in a 'one-shot' calculation for the corrected density of states (using the DFT-PBE converged charge density), an approach we refer to as DFT+Σ.

Evaluating the extent of charge transfer

To evaluate the extent of charge transfer, we consider the energy levels of the lowest unoccupied molecular orbital (LUMO). The LUMO is not coupled to the Au states, and its position therefore serves as an indicator of the local electrostatic potential at the molecule. We find that the LUMO position for the adatom binding site is 0.24 eV further from E_{Fermi} than for clean Au(111), indicating that more electronic charge is transferred from BDA to Au in the adatom case. This is consistent with the stronger binding observed at undercoordinated sites, as well as the difference in HOMO positions at the DFT-GGA level.

References.

1. Cvetko, D.; Lausi, A.; Morgante, A.; Tommasini, F.; Prince, K. C.; Sastry, M. *Measurement Science & Technology,* **1992,** 3, (10), 997-1000.
2. Floreano, L.; Naletto, G.; Cvetko, D.; Gotter, R.; Malvezzi, M.; Marassi, L.; Morgante, A.; Santaniello, A.; Verdini, A.; Tommasini, F.; Tondello, G. *Review of Scientific Instruments,* **1999,** 70, (10), 3855-3864.
3. Ho, K. M.; Bohnen, K. P. *Physical Review Letters,* **1987,** 59, (16), 1833-1836.
4. Franziska Traeger. *ChemPhysChem,* **2006,** 7, (5), 1006-1013.
5. Safron, S. A.; Duan, J.; Bishop, G. G.; Gillman, E. S.; Skofronick, J. G. *The Journal of Physical Chemistry,* **2002,** 97, (9), 1749-1757.
6. Venkataraman, L.; Park, Y. S.; Whalley, A. C.; Nuckolls, C.; Hybertsen, M. S.; Steigerwald, M. L. *Nano Letters,* **2007,** 7, (2), 502-506.
7. Venkataraman, L.; Klare, J. E.; Nuckolls, C.; Hybertsen, M. S.; Steigerwald, M. L. *Nature,* **2006,** 442, (7105), 904-907.
8. Venkataraman, L.; Klare, J. E.; Tam, I. W.; Nuckolls, C.; Hybertsen, M. S.; Steigerwald, M. L. *Nano Letters,* **2006,** 6, (3), 458 - 462.
9. Jones, R. O.; Gunnarsson, O. *Reviews of Modern Physics,* **1989,** 61, (3), 689.
10. Neaton, J. B.; Hybertsen, M. S.; Louie, S. G. *Physical Review Letters,* **2006,** 97, (21), 216405.
11. Quek, S. Y.; Venkataraman, L.; Choi, H. J.; Loule, S. G.; Hybertsen, M. S.; Neaton, J. B. *Nano Letters,* **2007,** 7, (11), 3477-3482.
12. Quek, S. Y.; Choi, H. J.; Louie, S. G.; Neaton, J. B. *Nano Letters,* **2009,** 9, (11), 3949-3953.
13. Frisch, M. J.; Trucks, G. W.; Schlegel, H. B.; Scuseria, G. E.; Robb, M. A.; Cheeseman, J. R.; Montgomery, J., J. A.; Vreven, T.; Kudin, K. N.; Burant, J. C.; Millam, J. M.; al, e. *Gaussian, Inc., Wallingford CT, 2004.*
14. Becke, A. D. *Journal of Chemical Physics,* **1993,** 98, (7), 5648-5652.
15. Lee, C. T.; Yang, W. T.; Parr, R. G. *Physical Review B,* **1988,** 37, (2), 785-789.